Cerebral Cortex September 2015;25:3182–3196
doi:10.1093/cercor/bhu111
Advance Access publication June 5, 2014

Local and Global Correlations between Neurons in the Middle Temporal Area of Primate Visual Cortex

Selina S. Solomon[1,2], Spencer C. Chen[1,2], John W. Morley[3] and Samuel G. Solomon[1,2,4]

[1]ARC Centre of Excellence in Vision Science, Sydney, NSW, Australia, [2]Discipline of Physiology, School of Medical Sciences and Bosch Institute, The University of Sydney, Sydney, NSW 2006, Australia, [3]School of Medicine, University of Western Sydney, Campbelltown, NSW 2560, Australia and [4]Department of Experimental Psychology, University College London, WC1P 0AH, UK

Address correspondence to Selina S. Solomon, Discipline of Physiology, School of Medical Sciences and Bosch Institute, The University of Sydney, NSW 2006, Australia. Email: selina@physiol.usyd.edu.au

In humans and other primates, the analysis of visual motion includes populations of neurons in the middle-temporal (MT) area of visual cortex. Motion analysis will be constrained by the structure of neural correlations in these populations. Here, we use multi-electrode arrays to measure correlations in anesthetized marmoset, a New World monkey where area MT lies exposed on the cortical surface. We measured correlations in the spike count between pairs of neurons and within populations of neurons, for moving dot fields and moving gratings. Correlations were weaker in area MT than in area V1. The magnitude of correlations in area MT diminished with distance between receptive fields, and difference in preferred direction. Correlations during presentation of moving gratings were stronger than those during presentation of moving dot fields, extended further across cortex, and were less dependent on the functional properties of neurons. Analysis of the timescales of correlation suggests presence of 2 mechanisms. A local mechanism, associated with near-synchronous spiking activity, is strongest in nearby neurons with similar direction preference and is independent of visual stimulus. A global mechanism, operating over larger spatial scales and longer timescales, is independent of direction preference and is modulated by the type of visual stimulus presented.

Keywords: area MT, extrastriate, marmoset, population coding, visual motion

Introduction

Cortical neurons show variable firing rate, and some of this variability is shared with other neurons. This co-variability, also called "noise correlation", arises in neurons that share input or are reciprocally connected (Moore et al. 1970; Nowak et al. 1995; Shadlen and Newsome 1998). Knowledge of how noise correlations are distributed is therefore important to understand the circuitry of neuronal populations, and in clarifying the signals that these populations provide. A productive focus of empirical and theoretical research has been the visual system, where perceptual work has clarified the requirements of population codes, and the receptive field properties of cortical neurons are well described. The relationship between perceptual decisions and correlated variability has been most thoroughly explored in area middle-temporal (MT) of the primate visual cortex (Newsome et al. 1989; Salzman et al. 1990; Britten et al. 1992)—an extrastriate area that is highly conserved among different primate species and is important in motion vision and the control of eye movements (Newsome and Pare 1988; Priebe and Lisberger 2004; Huang and Lisberger 2009). Work in macaque monkey shows that noise correlations have marked influence on fine motion discriminations and help yoke the activity of individual neurons to trial-by-trial fluctuations in perceptual judgments about the same stimulus (Zohary et al. 1994; Shadlen and Newsome 1998).

The spatial and temporal scales of spike correlations have now been well characterized in the primary visual cortex (V1) of macaque monkey and cat (van Kan et al. 1985; Hata et al. 1991; Nelson et al. 1992; Snider et al. 1998; Reich et al. 2001; Kohn and Smith 2005; Smith and Kohn 2008). Much less is known about extrastriate visual areas. There are good reasons to believe that the spatial and temporal scales of correlations in extrastriate areas may be different from that in V1. First, receptive fields in extrastriate areas are usually much larger than those in V1, implying substantial convergence of afferent input. Second, the major feed-forward input to V1 arises in the lateral geniculate nucleus (LGN), but extrastriate areas draw feed-forward input from other cortical areas, including V1, as well as subcortical areas (Weller et al. 1984; Sincich et al. 2004; Born and Bradley 2005; Nassi et al. 2006; Lyon et al. 2010; Warner et al. 2010). Third, indirect comparisons suggest that spike correlations are more pronounced in V1 than in extrastriate cortex (Gu et al. 2011; Chen et al. 2013; Liu et al. 2013; Smith and Sommer 2013; Smith et al. 2013).

The objective of this study was to establish the spatial and temporal structure of noise correlations in area MT. To do this, we made multi-electrode recordings from area MT of marmoset, a diurnal New World monkey in which area MT lies exposed on the cortical surface. The functional properties of neurons in the LGN (White et al. 2001; Solomon et al. 2002), V1 (Yu et al. 2010; Cheong et al. 2013), and area MT (Rosa and Elston 1998; Solomon et al. 2011) of marmoset are qualitatively and quantitatively similar to those of Old World macaque monkey. We first characterize the spatial and temporal structure of noise correlations between pairs of single neurons and show its stimulus dependence. We then extend the analysis to estimate noise correlations across populations of neurons. Together these analyses suggest 2 distinct mechanisms underlying noise correlations in area MT—one that is independent of stimulus and prominent over short timescales and one that is slower and stimulus dependent. Comparison of noise correlations in area MT and area V1 suggests that processing within area MT reduces noise correlations and contributes to dependence on visual stimulus.

Materials and Methods

Ethical Approval

Ten adult marmosets (*Callithrix jacchus*; 7 males; weight 290–400 g) were obtained from the Australian National Health and Medical Research Council (NHMRC) combined breeding facility. Procedures were

approved by Institutional (University of Sydney) Animal Ethics Committee and conform to the Society for Neuroscience and NHMRC policies on the use of animals in neuroscience research.

Experimental Preparation

Each animal was initially sedated with an intramuscular (IM) injection of 12 mg/kg of Alfaxan and 3 mg/kg of Diazepam. We then gave preoperative IM injections of 0.2 mg/kg of atropine (Pfizer), to reduce lung secretions, and dexamethasone (0.3 mg/kg; Maine Pharmaceuticals) to reduce inflammation. Subsequent surgery was performed under supplemental local anesthesia (Lignocaine 2%; Astra Zaneca). A femoral vein was cannulated, the trachea exposed and an endotracheal tube inserted, and the animal placed in a stereotaxic frame. Post-surgical anesthesia was maintained by continuous intravenous infusion of sufentanil citrate (4–12 μg/kg/h; Sufenta Forte, Janssen Cilag) in physiological solution (sodium lactate, Baxter International) with added dexamethasone (0.4 mg/kg/h; Mayne Pharma) and Synthamin 17 (225 mg/kg/h; Baxter International). The electrocardiogram, electroencephalogram (EEG), and SpO_2 were monitored continuously. Dominance of low frequencies (1–5 Hz) in the EEG recording, and absence of EEG changes under noxious stimulus (tail pinch) were used as the chief sign of an adequate level of anesthesia. At any sign of the anesthesia becoming less effective, the dose of sufentanil citrate was increased. Muscular paralysis was then induced and maintained by continuous infusion of pancuronium bromide (0.3 mg/kg/h; Astra Zaneca). The animal was artificially ventilated, with a 70:30 mix of N_2O and Carbogen, so as to keep end-tidal CO_2 near 33 mm Hg. Rectal temperature was kept near 38°C with the use of a heating blanket. Additional antibiotic and anti-inflammatory cover was given daily by IM injection of 25 mg of Noricillin (Norbrook), and 0.1 mg of dexamethasone. The pupils were dilated with atropine sulfate, and the corneas were protected with high-permeability contact lenses that remained in place for the duration of the experiment. No artificial pupils were used. At the end of the experiment, the animal was euthanized with intravenous 500 mg/kg sodium pentobarbitone (Lethobarb; Verbac Australia). The animal was perfused transcardially with 0.9% sodium chloride and then 4% paraformaldehyde in 0.1 M phosphate buffer, following which the brain was removed and post-fixed for 24 h. The tissue was then transferred to a 30% sucrose solution in 0.1 M phosphate buffer.

Recordings

In 9 animals, a craniotomy was made over area MT. We identified the posterior tip of the lateral sulcus, then made a series of single-electrode penetrations anterior and lateral to that location, and used the presence of directionally tuned multi-unit activity to identify likely location of area MT. In 6 animals, a large durotomy was made and extracellular recordings were obtained using a 10 × 10 grid of parylene-coated platinum iridium microelectrodes (1.5 mm in length, spacing 0.4 mm; Blackrock Microsystems). The array was inserted to a depth of approximately 1 mm using a pneumatic insertion device (Rousche and Normann 1992). The surface curvature of the cortex in and around area MT means that the depth of the electrodes will vary with location in the cortex. Three of these implants were used to obtain separate recordings that have been reported elsewhere (McDonald et al., 2014). In 3 animals that were implanted with the 10 × 10 arrays, coronal sections (50 μm thick) were cut on a freezing microtome, and alternate sections were stained for Nissl substances with cresyl violet, or for myelin with Gallyas silver (Bourne et al. 2007). In these animals, the electrode tracks reached layers 4–6. We note that because insertion or removal of the array may extend the electrode tracks beyond the recording location, we cannot rule out the possibility that recordings were obtained from upper layers.

In 3 other animals, we made 12 insertions of an array (NeuroNexus) of 8 laminar probes (spacing 0.2 mm), each of which had 8 iridium contact points (spacing 0.2 mm). After making a small durotomy, the laminar probes were inserted near perpendicular to the cortical surface, to a depth of approximately 2 mm, until all contact points and the reference were within cortex. In an additional animal, we used the laminar probes to make 3 penetrations into V1 across 2 hemispheres; 1 in which we recorded from the exposed surface of V1, where receptive fields are parafoveal, and 2 where we inserted the probes deeper, toward the calcarine sulcus, to target peripheral V1 receptive fields; in these cases, receptive fields were near the horizontal meridian, around 15 degrees eccentricity. Signals from each contact point were amplified, bandpass-filtered (0.3–5 kHz), and digitized at a rate of 24 kHz by an RZ2 real-time processor (Tucker-Davis Technologies). Offline-analyses were performed using Matlab (MathWorks, Inc.) and Offline Sorter (Plexon, Inc.).

Visual Stimuli

Visual stimuli were drawn at 8-bit resolution using commands to OpenGL, by custom software (EXPO; P. Lennie) running on a G5 Power Macintosh computer. Stimuli were displayed on a calibrated cathode ray tube monitor (Sony G520, refresh rate 100 Hz, mean luminance 45–55 cd/m^2, width 40 cm and height 30 cm). The monitor was viewed at a distance of 114 cm via a front-silvered mirror (V1 recordings), or directly at 45 cm (MT recordings). We focused the eyes at the appropriate distance using supplementary lenses, the power of which was chosen to optimize the spatial resolution of parvocellular cells in the dorsal LGN of the thalamus, confirmed by measurements contralateral to the recording site. During measurements, 1 eye, usually the contralateral eye, was occluded.

In 1 stimulus set, white circular dots (Weber contrast 1.0; diameter 0.4 degrees) moved across the monitor; outside each dot, the monitor was held at the mean luminance. Dots were presented at a density of 0.3 dots/s/degree and moved with 100% coherence and infinite lifetime. The position of each dot at the beginning of a trial was specified by a random number generator; the same set of positions was used on every trial. In another set of stimuli, a large sine-wave grating (Michelson contrast 0.5) drifted within a circular window (MT: diameter 30 degrees; V1: diameter 14 degrees) with hard edges; outside the window, the luminance was held at the mean value. The spatial frequency was 0.2 cycles/degree, and temporal frequency was 4 or 5 Hz, except in 1 array recording from area MT where spatial frequency was 0.5 cycles/degree, and temporal frequency was 8 Hz. For both dot fields and gratings, different motion directions (90 degree steps) were presented in pseudorandom order for 2 s; between trials, the screen was held at the mean luminance for 2 s. We obtained responses to 100 trials of each stimulus.

To estimate the spatial receptive field of each electrode, we measured response to a dot field moving in each of 8 directions (45 degree steps) at each of 12 positions tiling the stimulus screen. Dot size and speed, and density of the dot field, were the same as that used above. Each of stimuli in the set, which included a blank screen, was presented in pseudorandom order for 0.50 s; between trials, the screen was held at the mean luminance for 0.05 s. We obtained responses to 20 trials of each stimulus.

Spike-Sorting and Analysis Criteria

When inserting the 10 × 10 array, we needed to position the array to ensure insertion was normal to the electrodes, and we took care to avoid major blood vessels. The consequence of these constraints is that not all electrodes were confined to area MT. We inspected the receptive field positions and directional-sensitivity of the (multi-unit) recordings at each electrode of the 10 × 10 array. In all implants, the majority of receptive fields were in the upper quadrant of the visual field. From the trajectory of receptive field positions (Rosa and Elston 1998), we were able to identify electrodes that were likely to be within area MT, and others likely to be in area MTc (a thin area that in our recordings bordered much of anterior MT). Of the 96 recording electrodes (4 electrodes are inactive), an average of 63.0% (range 40.6–87.5%) were classified as within area MT and 18.9% (range 10.4–33.3%) were classified as within area MTc. For the current analyses, we have included neurons from electrodes in both regions.

The function *findpeaks* in the Matlab environment was used to identify candidate waveforms with peak amplitude that exceeded 3 standard deviations (SDs) of the raw signal on the relevant channel. Subsequent classification of these waveforms was made using Plexon Offline Sorter. Single-unit waveforms were manually identified as clusters in principal component space. In all putative single-units, we

subsequently found less than 2% of the interspike intervals (ISIs) were under 1 ms. The great majority of units (93%) showed less than 1% of ISIs under 1 ms. To quantify the reliability of the spike sorting, we obtained the signal-to-noise ratio (SNR) of the spike waveform for each unit; the amplitude of the mean waveform normalized by twice the SD of the noise in the waveform (Nordhausen et al. 1996; Suner et al. 2005; Kelly et al. 2007). The SNRs are summarized in Table 1. The minimum SNR of units in our sample was 2.35; 2 neurons had SNR of <2.75 (Smith and Kohn 2008). We accepted all the putative single-units for further analysis.

In the following analyses, we only include units where response to the most effective stimulus direction was at least 1 spike/s greater than the maintained discharge, or the least effective direction, whichever was smaller. This allowed us to include those neurons that were visually driven around the maintained discharge. From 6 implantations of the 10 × 10 array into area MT, we identified 274 single-units from 8 dot field stimulus sets (in 2 animals, we made separate measurements during stimulation through the contralateral and ipsilateral eye), and 250 single-units from 5 grating stimulus sets, obtained from 4 animals. Of these units, 180 (dot fields) and 143 (gratings) passed the response criterion. For these analyses, we will incorporate knowledge of the preferred motion direction, so we imposed additional criteria to ensure the units were direction-selective: the response to the most effective stimulus direction was at least 1.5 times the response to the opposite direction, and at least 1 spike/s greater in magnitude. Imposing this criterion for direction-selectivity left 151 (dot fields) and 114 (gratings) single-units.

From penetrations of the laminar probes in area MT, we identified 137 single-units from 12 dot field stimulus sets, of which 92 passed the response criterion. From penetrations of the laminar probes into V1, we identified 69 (3 dot field data sets) and 68 (3 grating data sets) single-units. Of these, 62 and 55 passed the response criterion. When comparing results between area MT and area V1, we limit our analyses to recordings from laminar probes. We did not impose additional criteria for direction-selectivity because these analyses do not incorporate knowledge of preferred motion direction.

For recordings from the 10 × 10 arrays implanted into area MT, an average of 20 neurons (SD 14) in each data set passed all the relevant criteria. For laminar probes inserted into area MT, the average was 8 neurons (SD 6); for laminar probes inserted into area V1, the average was 20 neurons (SD 10). Table 1 summarizes peak response rate, and mean response over the 2 s, for the most effective stimulus, in those neurons that passed response criterion. For recordings from area MT, we obtained 1738 pairs (dot fields) and 1858 pairs (gratings) from the 10 × 10 array recordings, and 483 pairs from the laminar probes. For recordings from area V1, we obtained 756 pairs (dot fields) and 557 pairs (gratings).

Estimating Direction Preference

We estimated preferred direction from the vector sum of responses to equally spaced motion directions:

$$R = \frac{\sum_k \overline{N_k} e^{i\theta_k}}{\sum_k \overline{N_k}} \tag{9}$$

where $\overline{N_k}$ and θ_k are the mean spike count and the direction of motion for the kth direction. We extracted the preferred direction, θ_{pref}, from the angle of the vector R.

Estimating Receptive Field Separation

Multi-unit responses to the matrix of stimuli were subject to singular value decomposition (SVD) to obtain the weight given by each electrode to each spatial position. We then found the best predictions of a two-dimensional Gaussian model of the spatial receptive field (using the function *lsqcurvefit* in the Matlab environment). From these fits, we extracted the position and length of the major and minor axes of the elliptical surface that best described the spatial weights estimated by the SVD. For the current analyses, we define the radius of the receptive field as the average of the half-width-at-half-height along the major and minor axes. The distance between receptive fields of 2 electrodes is the Euclidean distance between the 2 centers, normalized by the geometric mean of the radii.

Estimating Spike Count Correlation between Pairs of Neurons

The spike count correlation (r_{SC}) is the Pearson correlation coefficient of the spike counts of 2 units to repeated presentations of the same stimulus: r_{SC} characterizes the co-variation in trial-to-trial response amplitude ("noise correlations"). The r_{SC} between a pair of neurons is as follows:

$$r_{SC} = \frac{E(N_1 \cdot N_2) - E(N_1) \cdot E(N_2)}{\sigma_{N1} \cdot \sigma_{N2}} \tag{1}$$

where N_1 and N_2 are the spike counts of each neuron, and E and σ are, respectively, the mean and SD of the spike counts. For the current analyses, we also established spike count correlation across all stimuli in the set. To do this, we first z-scored the spike counts so that response to each direction had mean of zero and unit variance. The process of z-scoring makes some terms in equation 1 irrelevant: the denominator takes on a value of 1, and the means for each neuron are zero. Equation 1 therefore reduces to:

$$r_{SC} = E(Z_1 Z_2) \tag{2}$$

where Z_1 and Z_2 are the z-scored spike counts of the 2 neurons. We used equation 2 to characterize spike count correlations during presentation of visual stimuli. Very slow fluctuations in for example physiological state can induce spike count correlations. In analyses not shown, we dissected the contribution of correlations with time course less than 50 s from those with longer time courses, using standard methods (Bair et al. 2001). These analyses showed that correlations with time courses longer than 50 s contributed less than 10% to our measurements of r_{SC}. We did not explore these slow correlations any further.

To establish any biases in measurement of r_{SC}, we first re-computed r_{SC} after shuffling trials. For data sets obtained from 10 × 10 array implants in area MT, this procedure returned mean r_{SC} of 0.0003 (dot fields; standard error of the mean [SEM] 0.0005) and −0.0002 (gratings; SEM 0.0004). The order of stimuli was identical across animals, so to assess possible effects of stimulus sequence, we next estimated r_{SC} for pairs of neurons drawn from different animals: average r_{SC} was 0.0010 (dot fields; SEM 0.0002) and 0.0037 (gratings; SEM 0.0003).

To characterize co-variation in maintained discharge rate, we measured spike count over the last 1 s of the blank gray screen between each stimulus presentation and calculated the Pearson's correlation coefficient using equation 1. These measurements are unlikely to be

Table 1
Isolation quality and response of single-units in area MT and area V1

Area	Array	Stimulus	Number of neurons	Waveform SNR	Mean response	Peak response
MT	10 × 10 array	Dot field	151	5.22 ± 1.19 (5.01)	3.67 ± 5.50 (2.08)	7.37 ± 9.95 (4.88)
MT	10 × 10 array	Grating	114	4.62 ± 1.07 (4.40)	2.71 ± 3.74 (1.54)	5.72 ± 6.87 (3.4)
MT	Laminar probe	Dot field	92	4.95 ± 0.71 (4.94)	4.07 ± 5.24 (2.56)	9.44 ± 12.9 (5.55)
V1	Laminar probe	Dot field	62	4.39 ± 0.74 (4.28)	9.70 ± 8.51 (5.81)	15.62 ± 16.7 (9.46)
V1	Laminar probe	Gratings	55	4.50 ± 0.82 (4.48)	7.52 ± 9.90 (4.12)	13.4 ± 22.9 (5.96)

Note: All cells show: mean ± SD (median). SNR: signal-to-noise ratio (see Materials and Methods). Response: response magnitude in spikes/s.

influenced by latent effects from visual stimulation: in separate analyses, we computed r_{SC} separately for period 1–1.5 s and 1.5–2 s after offset of visual stimuli. There was no significant difference in r_{SC} for the 2 time periods ($P = 0.32$, $n = 1738$ for measurements between dot fields, $P = 0.61$, $n = 1858$ between gratings), and no significant difference for measurements made between presentation of dot fields and presentation of gratings ($P = 0.49$). We report measurements from the last 1 s of the blank gray screen between presentations of gratings.

Single-units isolated from the same electrode are potentially susceptible to sorting errors that may in turn inflate or deflate measures of spike count correlation (Cohen and Kohn 2011). For pairs of neurons isolated from the same electrode, we therefore measured the dependence of r_{SC} on the proportion of ISIs shorter than 1 ms ("ISI violations"), the SNR and the stimulus presented using ANCOVA analysis. This revealed that the average proportion of ISI violations across a pair of neurons explained 3.4% of the variance in the measured r_{SC} ($P < 0.001$) and that the geometric mean SNR across a pair of neurons explained 2.6% of the variance in the measured r_{SC} ($P < 0.001$). We conclude that variations in spike sorting have little effect on the measurements of r_{SC}.

Estimating Cross-Correlograms

To characterize the time course of spike correlations, we made cross-correlograms (Bair et al. 2001) between the spike trains (bin width 1 ms) of each pair of neurons:

$$\mathrm{CCG}(t) = \frac{(1/M)\sum_{i=1}^{M}\sum_{t=1}^{N} x_1^i(t)x_2^i(t+\tau)}{\phi(\tau)\sqrt{\lambda_1\lambda_2}} \tag{3}$$

where M is the number of trials, N is the number of bins in each trial, $x_1^i(t)$ and $x_2^i(t)$ are spike trains of the 2 neurons on the i-th trial, τ is the time lag, and λ_1 and λ_2 are the mean firing rates (spikes/s) of the 2 neurons. ϕ is a triangular function that corrects for the overlap between the 2 spike trains and is given by:

$$\phi(t) = T - |t|,\ -T < t < T \tag{4}$$

where T is the duration of the spike train segments used to compute the cross-correlogram.

For analyses of correlations at all timescales, CCGs were corrected for stimulus-induced correlations by subtracting an all-way shuffle predictor, approximated by the equation:

$$\mathrm{CCG}(t)_{\mathrm{shuffle}} = \frac{(1/M)\sum_{i=1}^{M}\sum_{t=1}^{N} \mathrm{PSTH}_1^i(t)\mathrm{PSTH}_2^i(t+\tau)}{\phi(\tau)\sqrt{\lambda_1\lambda_2}} \tag{5}$$

where PSTH_1 and PSTH_2 are the peri-stimulus time histograms (bin width 1 ms) of the 2 neurons (Bair et al. 2001).

To quantify the magnitude of correlations at different timescales, we computed the metric r_{CCG} (Bair et al. 2001; see also Kohn and Smith 2005; Smith and Kohn 2008). This is the integral of the shuffle-corrected CCG divided by the geometric mean area of the shuffle-corrected auto-correlograms (ACG) of the 2 neurons:

$$r_{\mathrm{CCG}}(t) = \frac{\sum_{\tau=-t}^{t}\mathrm{CCG}(\tau)}{\sqrt{\left(\sum_{\tau=-t}^{t}\mathrm{ACG}_1(\tau)\right)\sum_{\tau=-t}^{t}\mathrm{ACG}_2(\tau)}} \tag{6}$$

where

$$\mathrm{CCG}(\tau) = \frac{1}{M}\sum_{i=1}^{M}\sum_{t=1}^{N} x_1^i(t)x_2^i(t+\tau) - \frac{1}{M}\sum_{i=1}^{M}\sum_{t=1}^{N}\mathrm{PSTH}_1^i(t)\mathrm{PSTH}_2^i(t+\tau) \tag{7}$$

$$\mathrm{ACG}(\tau) = \frac{1}{M}\sum_{i=1}^{M}\sum_{t=1}^{N} x_1^i(t)x_1^i(t+\tau) - \frac{1}{M}\sum_{i=1}^{M}\sum_{t=1}^{N}\mathrm{PSTH}_1^i(t)\mathrm{PSTH}_1^i(t+\tau) \tag{8}$$

To assess the distribution of fast correlations (synchrony), we performed a parallel analysis, in which we removed slow temporal correlations from the CCG using a jitter-correction method (Smith and Kohn 2008; Amarasingham et al. 2012). A jitter-correction term was estimated by resampling the original data sets, such that spike times were jittered within a small temporal window (the "jitter window"), as follows. Each trial was divided into non-overlapping jitter windows. For each trial and each jitter window, spikes in 1 trial were replaced with a randomly chosen spike from the same jitter window in another trial. The correction term was estimated by applying equation (3) to this resampled data set. This correction term includes correlations at all timescales longer than the jitter time window, and because it preserves the shape of the PSTH, it also captures modulations in firing rate due to the presentation of a stimulus. Jitter-corrected CCGs were computed by subtracting the jitter-correction term from the raw CCGs obtained via equation (3). The jitter-corrected CCGs, therefore, capture correlations over timescales up to the length of the jitter window (here, 0.05, 0.1, 0.2, 0.5 and 1 s).

Estimating Correlations between a Neuron and a Population of Neurons

We estimated the correlation of a single neuron with the entire population of neurons recorded simultaneously, by computing the Pearson's correlation coefficient between the spike count of the single neuron and the pooled spike counts of the population of neurons:

$$\rho = \frac{E(Z_T \cdot P) - E(Z_T)\cdot E(P)}{\sigma_{Z_T}\cdot\sigma_P} \tag{10}$$

where Z_T is the spike count of the target neuron z-scored within each stimulus, P is the pooled z-scored spike count of all other neurons in the population, and E and σ represent the means and SDs in each case. Two estimates of population response, P, were investigated. In the first analysis ("unweighted"), each neuron in a population was given equal weighting, so on each kth trial, the population response P_k is the sum of all z-scored spike counts on that trial:

$$P_k = \sum_{i\neq T} Z_{i,k} \tag{11}$$

In the second analysis ("r_{SC}-weighted"), the z-scored activity of each neuron was weighted by the measured spike count correlation (r_{sc}, eq. 2) with the target neuron:

$$P_k = \sum_{i\neq T}\left(r_{\mathrm{sc}_{T,i}} \times Z_{i,k}\right) \tag{12}$$

Statistical Tests

For all statistical evaluation of r_{SC}, we performed a Fisher's *r-To-Z* transformation to stabilize the variance and applied statistical tests to the Z-value. The formula is given by:

$$Z = \frac{1}{2}\,\mathrm{In}\left(\frac{1+r_{sc}}{1-r_{sc}}\right) \tag{13}$$

We report actual P-values where the relevant statistical tests returned $P > 0.001$; for all $P < 0.001$, we report the relevant value as $P < 0.001$.

Non-Linear Regression

We used the function *nlinfit* in the Matlab environment to fit our model equations to our data. To assess whether a coefficient was statistically significant, we measured the confidence intervals using the function *nlparci* and ensured that these intervals did not overlap with zero.

Results

Our major aim is to characterize the spatial and temporal structure of noise correlations between neurons in area MT and how these correlations depend on the visual stimulus. To do

this, we measured correlations during maintained activity, and during presentation of 2 widely used visual stimuli: a drifting grating and a moving dot field. For both gratings and dot fields, response of neurons in area MT is robust and tuned for motion direction (Fig. 1).

All the measurements we include here are obtained from well-isolated single-units. The insets in Figure 1*A*,*B* show the average extracellular waveforms associated with 2 neurons in area MT. The waveforms are consistent and well separated from the remaining activity on each electrode. The quality of spike isolation can be captured by the SNR of the waveform: for the neurons in Figure 1*A*,*B*, the ratio was 4.9 and 4.4. Table 1 summarizes the quality of spike isolation across neurons included here.

Correlations between Pairs of Neurons

Figure 2*A* indicates the structure of the data we have analyzed. A field of white dots moved across a gray background for 2 s, and between stimulus presentations, the monitor screen was held at the gray background. Each of the 60 rows shows the spiking activity of a single neuron in area MT, with each point representing a single spike (overlapping points are darker). Of the 60 neurons, 46 passed criteria (Materials and Methods, "Spike Sorting and Analysis Criteria") and were accepted for subsequent analyses. To study the magnitude of correlations, we computed the spike count correlation (r_{SC}), a widely used measure of trial-by-trial correlation across pairs of neurons. Its calculation is illustrated in Figure 2*B*, where the 4 marginal plots compare activity of a pair of neurons, during presentation of dot fields moving in each of 4 motion directions. For each motion direction, spike count was measured for each of 100 trials and the array of spike counts was transformed into *z*-scores. The Pearson's correlation coefficient, *r*, was used to capture the variability in *z*-scores that was shared by the 2 neurons. The total spike count correlation, r_{SC}, is the correlation coefficient of *z*-scores collapsed over all motion directions (Fig. 2*B*, middle).

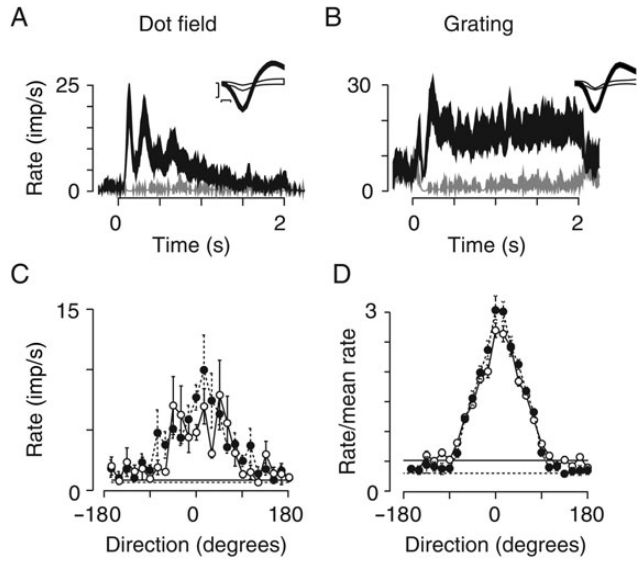

Figure 1. Visual responses of neurons in area MT of marmoset recorded with 10 × 10 electrode array. (*A*) Peri-stimulus time histograms (PSTHs; bin width 10 ms) of response of representative neuron to moving dot fields (20 degree/s; dot diameter 0.4 degrees). Dark-filled trace shows average ±1 SEM of response to preferred stimulus over 100 trials. Light-filled trace shows same but for response to the opposite direction. Inset shows the average ±1 SD of spike waveform of the neuron (filled trace) and "multi-unit" activity on the same electrode (open trace). SNR of this waveform was 4.9. Scale bars are 0.1 ms (abscissa) and 0.1 mV (ordinate). (*B*) Response of another neuron to drifting gratings (0.2 cycles/degree, 4 Hz). Conventions as in (*A*) SNR of this waveform was 4.4. (*C*) Average response of MT neurons to moving dot fields (filled symbols; $n = 114$) and moving gratings (open symbols; $n = 151$). Responses are aligned such that the preferred direction is 0 degrees. Horizontal lines show average maintained discharge, obtained during measurements with dot fields (dashed line) or gratings (solid line). Error bars show ±1 SEM. (*D*) Average response of MT neurons to moving dot fields and moving gratings, when normalized to the mean response of each neuron across directions. Neurons and conventions as in (*C*).

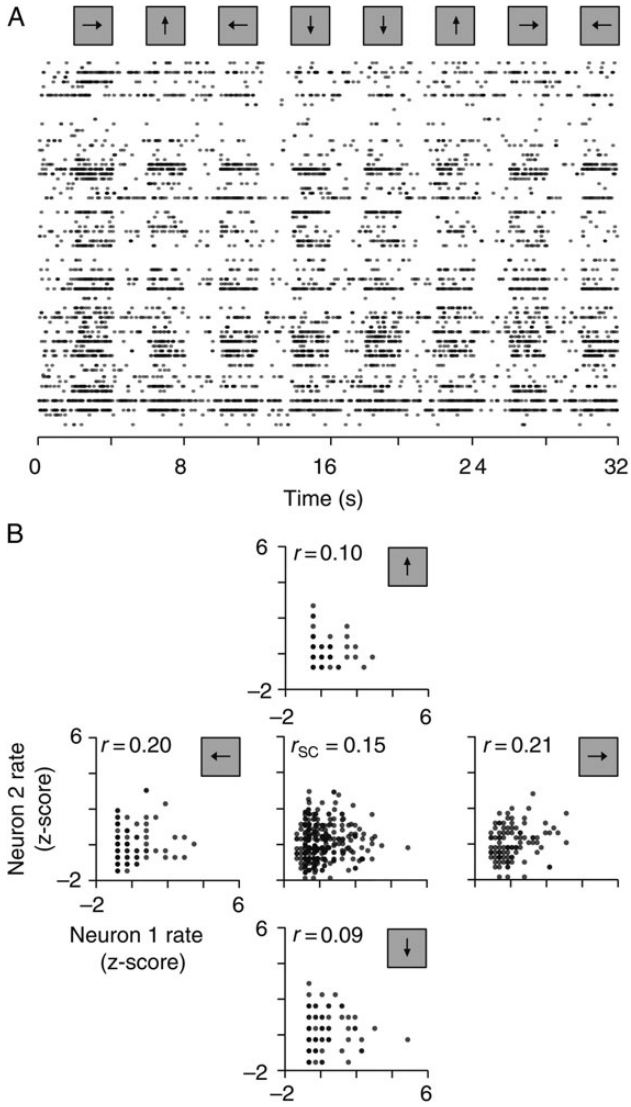

Figure 2. Illustrative data set and calculation of spike count correlations. (*A*) Raster plot of activity during presentation of a moving dot field, for 60 neurons obtained from 1 implantation of a 10 × 10 array into area MT of 1 animal (case MY147). Each row shows 1 single-unit, and each dot 1 spike from that neuron. Every 4 s a field of white dots moved over a background of the mean luminance for 2 s. Otherwise, the screen was held at the mean luminance. Arrows at the top indicate the motion direction of the dot field on each trial. (*B*) Calculation of spike count correlation. Response of each neuron to each motion direction was transformed into *z*-scores. The 4 marginal plots compare the *z*-scored response for 2 neurons, for each of 4 directions of motion as indicated by the arrows. The associated Pearson's correlation is shown in each plot. The center plot compares *z*-scored responses for the same 2 neurons, collapsed over all directions: the associated Pearson's correlation is the spike count correlation, r_{SC}.

Spike Count Correlations Decrease with Distance

Correlated variability in a pair of neurons implies that they share common input or are reciprocally connected. Nearby neurons are more likely to share inputs and connections, so we first established how spike count correlation (r_{SC}) depends on the distance between the electrodes that the 2 neurons were isolated from. Figure 3*A* shows mean r_{SC} as a function of cortical distance, during presentation of a moving dot field, a moving grating and a gray screen. To estimate r_{SC} for dot fields and gratings, we analyzed activity during the 1.0-s period that followed onset of a visual stimulus. To estimate r_{SC} for a gray screen, we analyzed activity during a 1.0-s period that started 1 s after offset of visual stimulus. Figure 3*A* makes 2 points. First, r_{SC} declines with distance and appears to be asymptotic for separations over 1.6 mm (gray screen: $P = 0.42$; dot fields: $P = 0.48$; gratings: $P = 0.11$, ANOVA). Second, r_{SC} is lower during presentation of a visual stimulus than during presentation of a gray screen and is lower for dot fields than gratings. For pairs of neurons separated by more than 1.6 mm, mean r_{SC} for dot fields was 0.029 (SEM 0.002) and that for gratings was 0.060 (SEM 0.002). For distances greater than 1.6 mm, mean r_{SC} during presentation of a gray screen was 0.066 if measured between presentations of dot fields and 0.074 if measured between presentations of gratings; these were not significantly different ($P = 0.129$, Student's *t*-test). This global positive r_{SC} does not reflect a bias introduced by our analyses and recording techniques: mean r_{SC} at large distances was substantially higher than that for artificial pairs ($P < 0.001$; see Materials and Methods, "Measurements of spike count correlation").

The receptive fields of neurons in area MT are organized into a retinotopic map, so distance between electrodes should be closely related to spatial overlap between receptive fields. In separate measurements, we estimated the spatial receptive field at each electrode. We characterized spatial overlap for each pair of electrodes as the distance between the centroids of the 2 receptive fields, normalized by the average size of the 2 receptive fields. This index, which we call RF separation, has a value of 0 when receptive fields are centered at the same point; a value of 2 indicates 2 receptive fields separated by their average diameter (at half-height), as illustrated by the inset in Figure 3*B*. Pairs of neurons separated by more than 1.6 mm are unlikely to show substantial receptive field overlap. This suggests that the decline in r_{SC} with cortical distance reflects reduced spatial overlap in receptive fields: a cortical distance of 1.6 mm is near that where r_{SC} approaches an asymptotic value (Fig. 3*A*).

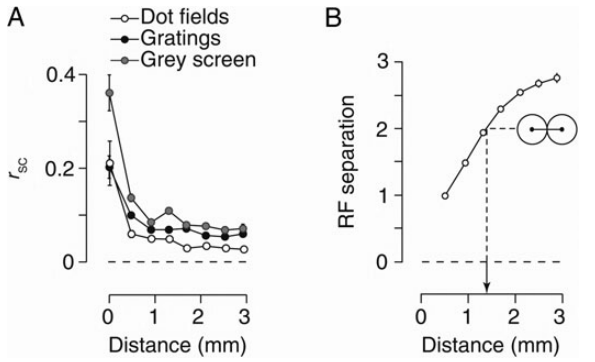

Figure 3. Spike count correlation (r_{SC}) decreases with distance. (*A*) Mean r_{SC} as a function of the cortical distance between neurons, during responses to a moving dot field (open circles; $n = 1738$), moving grating (filled black circles; $n = 1858$), or a gray screen presented between trials of moving gratings (filled gray circles). Error bars show ±1 SEM and are often smaller than the symbols. We were conservative when isolating single-units and identified 18 (dot fields) or 43 (gratings) pairs of neurons from a single electrode. Values at cortical distances greater than 0 are obtained from an average of 253 pairs (range 110–360). (*B*) Mean receptive field (RF) separation between pairs of electrodes ($n = 12\,528$), as a function of cortical distance. Calculation of RF separation is described in Materials and Methods. Inset shows representation of a pair of receptive fields that are circular and equal in diameter, which touch but do not overlap.

The above analysis showed that correlation strength depends on the cortical distance between neurons. In separate recordings, we asked whether distance tangential to the cortical surface has different impact than distance normal to the cortical surface. To establish this, we inserted an array of laminar probes approximately perpendicular to the cortical surface of area MT. We know that the electrodes were approximately perpendicular because neurons recorded on the same probe (spanning different layers) were more likely to have the same preferred motion direction, but the preferred directions of neurons on neighboring probes showed no relationship (not shown). We compared correlations for pairs of neurons recorded at the same depth ($n = 87$), and pairs of neurons recorded in the same column ($n = 59$). r_{SC} decayed with distance in both cases (not shown) but did not depend on whether pairs were at the same depth, or in the same column (dot fields: $P = 0.21$; gray screen: $P = 0.14$; ANOVA). We conclude that while correlation strength may depend on laminar and columnar position, the effect is subtle.

In summary, correlations in area MT decrease with distance: strong correlations are found locally, among neurons whose receptive fields show substantial spatial overlap. These local correlations are superimposed on global correlations that may extend across all of area MT and are reduced in the presence of a stimulus; this reduction is greater for moving dot fields than moving gratings.

Spike Count Correlations Depend on Direction Tuning and Stimulus Direction

We now show that spike count correlation in area MT can depend on preferred motion direction as well as cortical separation. To capture potential effects at longer timescales, in the following analyses, we compute r_{SC} over the entire 2-s period of visual stimulation. Figure 4*A* shows r_{SC} during presentation of moving dot fields, for pairs with similar direction preference (<45 degrees apart) and pairs with very different direction preference (more than 135 degrees apart). r_{SC} is greater for neurons with similar preferred direction, for cortical distances up to 1.2 mm. Pairs of neurons with intermediate direction difference had r_{SC} intermediate to these 2 curves (not shown). Figure 4*B* shows analogous plots during presentation of a moving grating: r_{SC} for gratings shows less dependence on the direction preference, and the curves differ only for distances up to 0.4 mm. Estimates of r_{SC} during presentation of a gray screen showed similar dependence on direction preference for distances up to 0.4 mm (not shown).

When neurons have very different preferred directions, there is no single motion direction that strongly drives both neurons. Dependence of spike count correlation on direction preference may therefore be confounded by differences in spike rate (de la Rocha et al. 2007; Cohen and Kohn 2011). To address this, we estimated r_{SC} for the stimulus direction

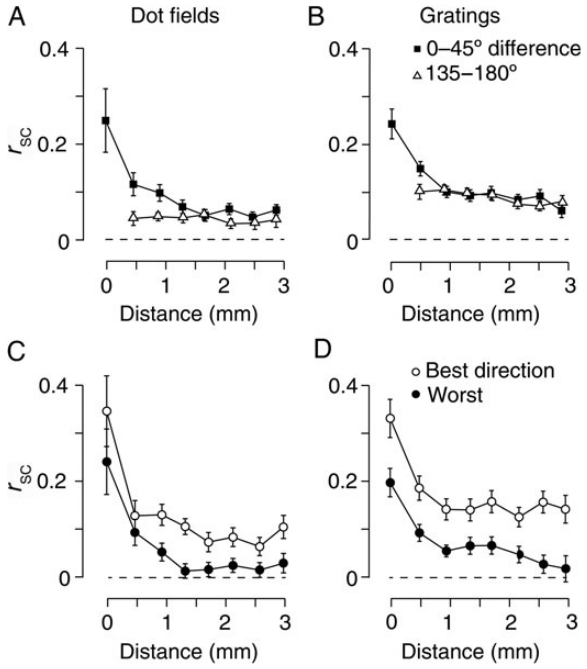

Figure 4. Spike count correlation depends on preferred motion direction and stimulus direction. (*A*) Mean r_{SC} during presentation of moving dot fields, for pairs of neurons with similar direction preference (squares, $n = 434$) and different direction preference (triangles, $n = 417$). Error bars show ±1 SEM. (*B*) Mean r_{SC} during presentation of a moving grating (similar direction preference, $n = 476$; different direction preferences $n = 470$). Conventions as in (*A*). (*C*) Mean r_{SC} during presentation of moving dot fields, for pairs of neurons with similar preferred motion direction (<45 degrees apart; $n = 434$). Open symbols show r_{SC} for the most effective motion direction; closed symbols show r_{SC} for the least effective motion direction. Error bars show ±1 SEM. (*D*) Same as (*C*) but during presentation of a moving grating ($n = 476$). Conventions as in (*C*).

associated with lowest geometric mean response, for pairs of neurons with preferred directions less than 45 degrees apart, or more than 135 degrees apart. In this analysis, pairs of neurons in both groups are poorly driven. For moving dot fields and pairs of neurons separated by up to 1.2 mm, r_{SC} was higher for similarly tuned pairs than for pairs with dissimilar tuning (0.10 vs. 0.06; $n = 130$ and 126, respectively; $P = 0.036$, one-tailed Students' *t*-test). For moving gratings and pairs of neurons separated by up to 0.4 mm, r_{SC} was also higher for similarly tuned pairs (0.14 vs. 0.08; $n = 70$ and 31, respectively; $P = 0.048$). These differences remained if we instead examined stimuli that evoked the lowest response across either of the neurons in the pair (dot fields: $P = 0.004$, gratings: $P < 0.001$).

Spike count correlations were nevertheless modulated by stimulus motion direction. To illustrate this, Figure 4*C*,*D* shows r_{SC} for pairs of neurons with preferred directions less than 45 degrees apart. For clarity, we show correlations during presentation of the stimulus direction nearest to the average preferred direction and the opposite direction; r_{SC} for intermediate stimulus directions was always intermediate to these. r_{SC} is higher when the stimulus moves in a direction close to that preferred by the pair of neurons. For both preferred and non-preferred motion directions, r_{SC} is higher for gratings than dot fields. Responses to the preferred motion direction are naturally larger than that to the opposite direction, and the dependence of r_{SC} on stimulus motion direction could simply reflect the dependence on firing rates. We therefore performed an ANCOVA to assess the dependence of r_{SC} on firing rates of the 2 neurons, preferred or opposite stimulus direction, and distance between neurons. This analysis revealed that the higher r_{SC} for preferred motion direction includes a dependence on stimulus direction in addition to the rate dependence ($P < 0.001$).

In summary, these analyses show that correlations are stronger in pairs of neurons that have similar direction tuning and overlapping receptive fields. In addition, global correlations span similarly and differently tuned neurons and are stronger during presentation of gratings than dot fields. For both dot fields and gratings, r_{SC} depends on stimulus direction and is highest for the preferred stimulus.

Modeling of Spike Count Correlation

The distribution of spike count correlations could be well described by a model incorporating the distance between neurons and the difference in their preferred direction, such that:

$$r_{SC} = A \times (e^{-\text{distance}/a})(1 - b \times \Delta\text{pref}_{dir}) + \text{offset} \qquad (14)$$

where A is gain in correlation, a is cortical space constant (the distance at which r_{SC} falls by 1/e), b is rate of r_{SC} decay with difference in preferred direction, and Δpref_{dir} is the difference in the preferred direction between the pair of neurons, in degrees. We used non-linear regression to find the parameters that best predicted r_{SC}. Cortical distance and difference in preferred direction were significant contributors to r_{SC} ($P < 0.05$) but not RF separation: this presumably reflects the fact that our estimates of cortical distance are more precise than our estimates of RF separation. The parameter values are provided in Table 2. For pairs of neurons with similar direction preferences (Fig. 4*C*,*D*), we repeated the regression, including now the stimulus direction, such that:

$$r_{SC} = A \times (e^{-\text{distance}/a})(1 - b \times \Delta\text{pref}_{dir}) - c \times \Delta\text{stim}_{dir} + \text{offset} \qquad (15)$$

where c is the rate of r_{SC} decay with relative stimulus direction, and Δstim_{dir} is the direction of the stimulus relative to the average preferred direction of the pair of neurons (Table 2).

Timescales of Pair-Wise Correlations

r_{SC} is a measure of correlation strength over the entire duration of the stimulus and does not distinguish between correlations occurring at different timescales. In the following, we address the temporal structure of correlations over the course of a trial. Our aim is to determine whether correlations arise from

Table 2
Quantitative models of spike count correlations in area MT

Model	Stimulus	Parameters				
Equation 14		A	a	b	offset	
	Dot field	0.21	0.66	0.0058	0.042	
	Grating	0.19	0.47	0.0043	0.083	
	Gray screen	0.32	0.35	0.0037	0.078	
Equation 15		A	a	b	c	offset
	Dot field	0.21	0.66	0.0058	0.00017	0.058
	Grating	0.19	0.47	0.0042	0.00039	0.12

coordinated neuronal activity that is tightly locked in time (synchrony), or slower co-variations. To characterize the timescales of correlations, we estimated cross-correlograms (CCGs) for each pair of neurons (see Materials and Methods). In 1 analysis, we computed conventional "shuffle-corrected" CCGs. We also computed "jitter-corrected" CCGs, which allow us to isolate correlations arising over shorter timescales.

Correlations at All Timescales Decay with Distance

Figure 5 shows average shuffle-corrected CCGs as a function of cortical distance, during presentation of a moving dot field, a moving grating, or a gray screen. Proximal pairs of neurons show a sharp peak with width 50–100 ms, superimposed on a broader hump with width of several hundred milliseconds. During presentation of dot fields, both the sharp peak and broad hump disappear at distances greater than 2 mm, but during presentation of gratings, they remain visible at the largest distance measured. CCGs obtained during presentation of a gray screen show larger and broader humps, indicating that slow correlations are more pronounced. The difference in CCGs obtained during presentation of a gray screen and gratings is larger than that expected from the difference in spike count correlation for these stimuli (r_{SC}; Fig. 3*A*). This is because, following Bair et al. (2001), we present CCGs that have not been normalized to the ACGs of the constituent neurons. In contrast, r_{SC} is equivalent to the area of the CCG, divided by the average area of the ACGs. Indeed, the ACGs obtained during presentations of a gray screen were larger than those obtained during presentations of a grating (not shown). We think that the larger ACGs found during presentation of a gray screen reflect slow rhythms in maintained activity that are disrupted during visual stimulation.

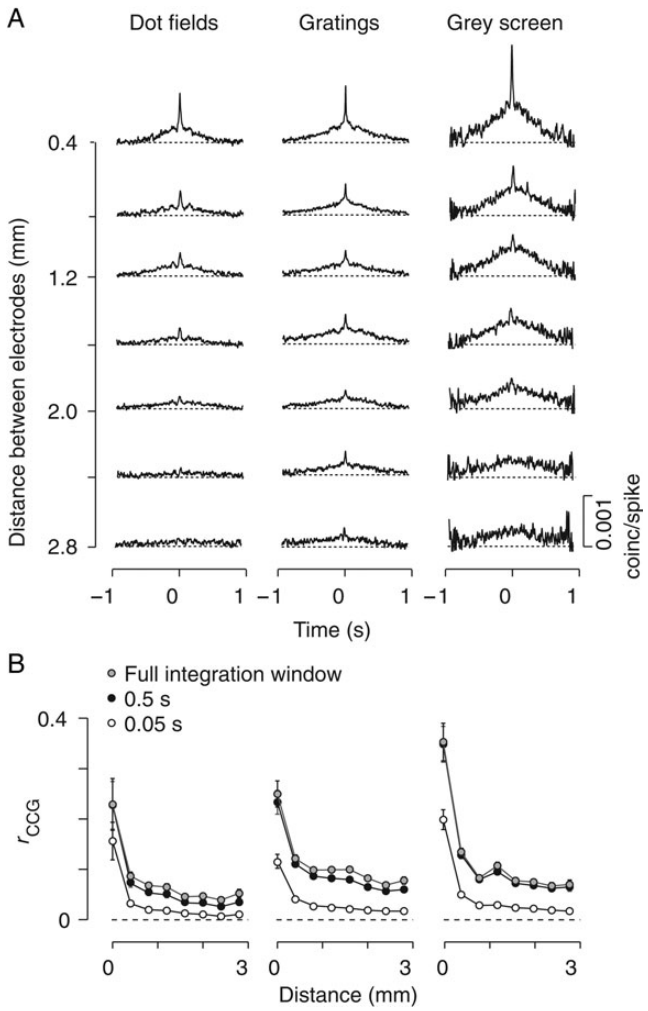

Figure 5. Correlations at all timescales decay with distance. (*A*) Shuffle-corrected cross-correlograms (CCGs) as a function of distance. CCGs were computed over 2 s during presentation of moving dot fields (left, $n = 1858$), or moving gratings (middle, $n = 1738$). CCGs in the right column were computed over the 1 s of gray screen presented between successive trials of moving gratings ($n = 1738$). For display purposes, CCGs were smoothed with a Gaussian filter (SD 0.005 s). (*B*) Mean r_{CCG} as a function of distance, for integration windows of 0.05 s (open circles), 0.5 s (black circles) or the maximum achievable integration window (gray circles). This was 2 s for dot fields (left) or gratings (middle) and 1 s for the gray screen (right). Same neurons as (*A*). Error bars show ±1 SEM.

To provide a quantitative analysis of the shuffle-corrected CCGs, we computed r_{CCG} (Bair et al. 2001), the integrated strength of correlation over a particular time window. For an integrating window of 2 s, r_{CCG} is equivalent to r_{SC}, as both metrics measure the strength of correlations occurring over the entire duration of a trial. Figure 5*B* shows r_{CCG} as a function of distance during presentation of a dot field (left panel) or grating (middle panel), for integration windows of 0.05, 0.5 and 2 s. Correlations at all timescales decay with distance. Figure 5*B* also shows that larger r_{SC} during presentation of gratings than dot fields primarily reflects correlations over longer timescales (hundreds of milliseconds); correlations at shorter timescales (0.05 s) are similar for both stimuli. Similarly, correlations at timescales less than 0.05 s are similar during visual stimulation or presentation of a gray screen: reduced r_{SC} during visual stimulation primarily reflects reduction in correlations over longer timescales.

Sharp peaks around time zero in the average shuffled-corrected CCGs (Fig. 5*A*) indicate that neurons are likely to fire synchronously. The amplitudes of the shuffled-corrected CCGs at these time lags, however, reflect contributions from both fast and slow correlations. To isolate correlations at short timescales, we calculated "jitter-corrected" CCGs, with varying jitter windows (Materials and Methods). Figure 6*A* shows the jitter-corrected CCGs as a function of cortical distance, for jitter windows of 0.05 s (black curves) and 0.5 s (gray curves). Jitter windows of 0.05 s yield similar CCGs regardless of whether the stimulus was a dot field, grating, or gray screen. In each case, CCG height decays with distance and peaks disappear beyond about 1 mm. Jitter windows of 0.5 s, however, yield different pattern of CCGs: peaks in these CCGs also decay with distance, but while they disappear above 2 mm during presentation of moving dot fields or gray screens, they extend at least 2.8 mm during presentation of gratings.

In summary, the strength of correlations at short timescales (up to 0.05 s) is similar during presentation of dot fields, gratings, and gray screens. Stimulus-dependent noise correlations are mainly due to correlations that emerge at timescales above 0.05 s.

Time Scales of Correlation and Direction Preferences

We showed above that r_{SC} can depend on preferred motion direction, at least among nearby neurons. In the following, we establish the timescales over which this dependence arises. Figure 7*A* shows average shuffle-corrected CCGs for

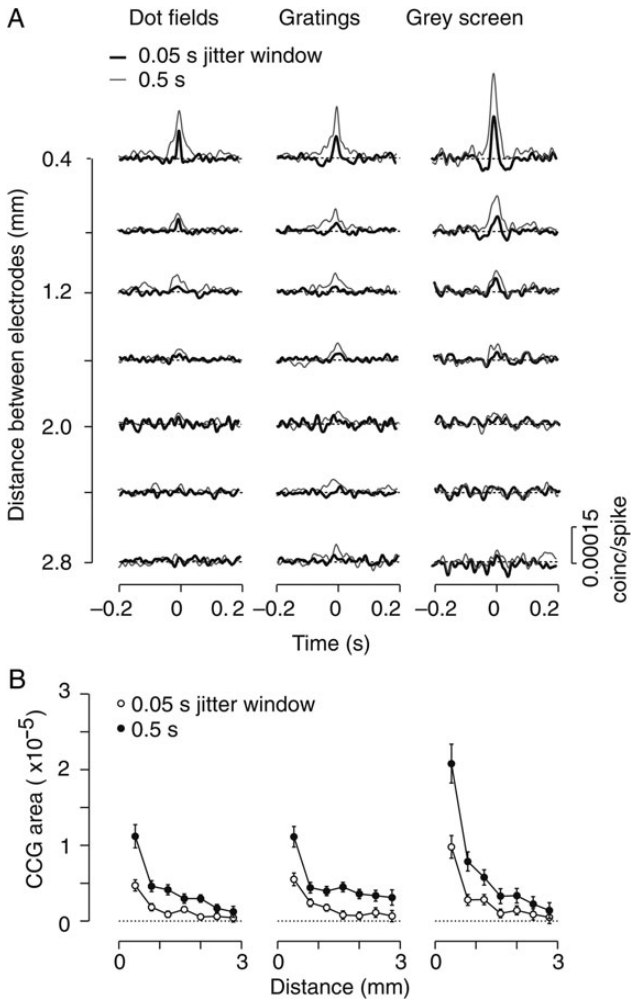

Figure 6. Near-synchronous activity is confined to nearby neurons. (*A*) Mean jitter-corrected CCGs, for jitter windows of 0.05 s (black) and 0.5 s (gray) during presentations of moving dot fields (left), moving gratings (middle), or a gray screen (right column). Same neurons as Figure 5*A*. (*B*) Mean of area under the jitter-corrected CCGs (±0.01 s), for jitter windows of 0.05 s (open circles) and 0.5 s (filled circles). Same neurons as (*A*). Error bars show ±1 SEM.

pairs of neurons with similar and different preferred direction, during presentation of dot fields; similarly tuned pairs show stronger CCGs, with larger peaks and broad humps. Figure 7*B* shows that for pairs of neurons with similar preferred direction, r_{CCG} declines rapidly with distance, at all timescales. In contrast, r_{CCG} is low and shows little distance dependence, in pairs of neurons with different preferred direction. Figure 7*C*,*D* shows similar analyses, but during presentation of gratings. Pairs of neurons with similar preferred direction show stronger CCGs and larger r_{CCG} for distances up to 0.4 mm, as was the case for r_{SC}.

Analysis of the CCGs made with the jitter-correction method confirmed that near-synchronous activity was approximately twice as strong in nearby pairs of neurons with similar preferred direction compared with those with different preferred directions (ANOVA, $P = 0.01$) but did not depend on whether the stimulus was a grating or dot field ($P = 0.55$). We also compared CCGs for each stimulus direction, as a counterpart to the analyses shown in Figure 4*C*,*D* (not shown). The shapes of the CCGs for the most effective and least effective stimulus directions were very similar, but CCGs for the most effective stimulus direction were enhanced at all timescales.

Population Covariance

Our analyses have so far considered noise shared between pairs of neurons, but even weak pair-wise correlations can be associated with substantial co-variability in populations of neurons (Chen et al. 2006). This is partly because the estimated magnitude of pair-wise correlations is influenced by independent noise in the activity of individual neurons, and partly because pair-wise correlations do not capture many aspects of higher-order co-variations among networks of neurons. To assess how variability is correlated among populations of neurons, we developed a novel measure that we call "population covariance" (see Materials and Methods). Population covariance is the correlation between the trial-by-trial activity of a single target neuron, and the pooled response of all other neurons simultaneously recorded; on each trial, the estimate of population activity is a weighted sum of *z*-scored activity across those neurons. This pooled population activity emphasizes the variability in spiking activity that is shared across a population, which is only partially captured in our pair-wise measurements of spike count correlation, r_{SC}. In Supplementary Material, we show the mathematical relationship between the population covariance and r_{SC}. As mentioned earlier, our analyses are confined to the first 1 s of stimulus-evoked activity, and the last 1 s of maintained activity.

We first measured population covariance when we gave equal contribution of each neuron to the pool (eq. 11), thereby ignoring the identity of the neurons in the comparison population. Population covariance was on average 0.25 during presentation of a gray screen; as for measurements of pair-wise correlations, population covariance was reduced during presentation of a visual stimulus (Fig. 8*A*; dot fields: 0.15, gratings: 0.22; $P < 0.001$, one-tailed paired Student *t*-test). The magnitude of pair-wise correlations depends on distance between neurons and their functional similarity. We incorporated the structure of pair-wise correlations by weighting the contribution of each neuron to the comparison population by its r_{SC} with the target neuron (eq. 12). Specifically, the weighting is provided by the r_{SC} calculated over the entire 1-s analysis window. The r_{SC}-weighting naturally refines the estimate of population activity, as viewed by the target neuron, and thereby increases the estimate of population covariance (Fig. 8*B*; dot fields: 0.33, grating: 0.38, gray screen: 0.39). These analyses demonstrate that although pair-wise correlations in area MT are generally low, covariance within populations of neurons can be substantial.

To establish the temporal structure of population covariance, we repeated the analyses above while varying the integration time window over which spike count was measured, with integration times from 0.005 to 1 s. For each integration time window, we divided trials into non-overlapping time bins of the appropriate width. For each successive time bin, we calculated the *z*-scored spike count across trials, separately for each stimulus direction, and thereby accounted for the shape of the PSTH in each neuron. We then collapsed across all possible time bins to compute the population covariance value for each integration time window. Figure 8*A*,*B* shows that population covariance increases with integration time window and

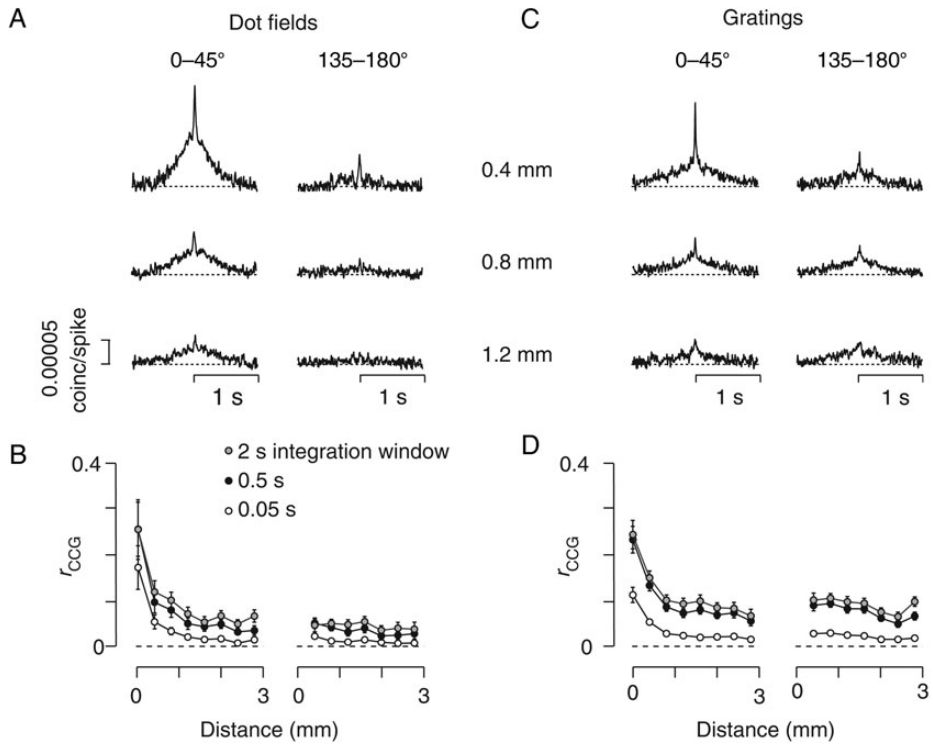

Figure 7. Dependence of correlations on preferred motion direction. (*A,B*) During presentations of moving dot fields. (*A*) Mean shuffle-corrected CCGs for pairs of neurons grouped according to the cortical distance between them (0.4, 0.8, or 1.2 mm) and by the difference in the preferred motion direction. (*B*) Mean r_{CCG} for integrating time windows of 0.05, 0.5, and 2 s as a function of cortical distance. Error bars show ±1 SEM. Same neurons as (*A*). (*C,D*) Same as (*A*) and (*B*) but during presentations of drifting gratings.

that the stimulus-evoked reduction in population covariance is most apparent for integration times greater than 0.05 s.

Comparison with Area V1

To provide normative data, we measured noise correlations in area V1 in 1 animal, making measurements during 3 penetrations of the laminar probes across 2 hemispheres. We compared these to measurements obtained from laminar probes inserted in area MT of different animals, and in the following include all possible pairs of neurons (average distance between neurons: MT, 0.71 mm; V1, 0.73 mm). Our aim was to establish the distribution of noise correlations in area V1 for direct comparison with area MT, so the parameters of the visual stimulus were those we used for recordings in area MT and were not optimized for neurons in area V1.

Figure 9*A–D* shows r_{SC} in area V1 and area MT; here we measure r_{SC} over 1-s period as done in Figure 3. The first observation is that r_{SC} is stronger in area V1 than area MT, whether for presentations of dot fields (0.18 vs. 0.04; $P < 0.001$, one-tailed Student *t*-test), or a gray screen (0.24 vs. 0.09; $P < 0.001$). In these experiments, the spike rate of neurons in area V1 was higher than that of neurons in area MT (Table 1). The higher r_{SC} in area V1, however, does not simply reflect the higher rate (de la Rocha et al. 2007; Smith and Kohn 2008; Cohen and Kohn 2011). This is shown by Figure 9*E,F*, which plots the relationship between r_{SC} and geometric mean rate for pairs of neurons in area V1 and area MT: r_{SC} is greater in area V1 than in area MT across the range of common firing rates. The same trends were seen if we ordered pairs by the minimum rate across the 2 neurons (not shown). Mean shuffle-corrected CCGs are provided as insets in Figure 9*A–D* and show that noise correlations at all timescales are stronger in area V1. The second observation is that r_{SC} in area V1 and area MT depends differently on visual stimulus. Above we showed that in area MT, r_{SC} is lowest for dot fields, highest for a gray screen, and that gratings provide intermediate values. In area V1, in contrast, average r_{SC} during presentation of gratings was 0.16 (SEM 0.01; $n = 557$; not shown), less than r_{SC} for dot fields or for a gray screen. This difference became more prominent over time: r_{SC} measured over 2 s of evoked activity increased to 0.26 during presentation of dot fields but remained 0.16 during presentation of gratings. Lower r_{SC} for gratings than dot fields in area V1 persisted when comparing pairs of neurons with similar geometric mean spike rates (not shown).

We considered the possibility that the reduction in noise correlation from area V1 to area MT was associated with changes in the spike rate variability of individual neurons. To assess this, we measured the ratio of variance to mean (Fano Factor) of individual neurons. Response to dot fields showed lower variability than response to gratings in area V1 (geometric mean Fano Factor: 2.63 vs. 3.66, $n = 62$ and 55; $P < 0.01$; one-tailed Student's *t*-test on log-transformed Fano Factors). The lower variability for dot fields is not surprising, as response of V1 neurons to dot fields was generally sparse, with epochs of high firing rates as single dots traversed the receptive field (not shown). In these conditions, variability is expected to be low (Muller et al. 2001). In contrast, responses of V1 neurons to gratings were generally sustained and elevated throughout the trial. In area MT, variability of response was similar for dot fields and gratings (Fano Factors 2.17 vs. 2.29, $n = 151$ and 114; $P = 0.24$), Fano Factors for neurons in area MT are lower

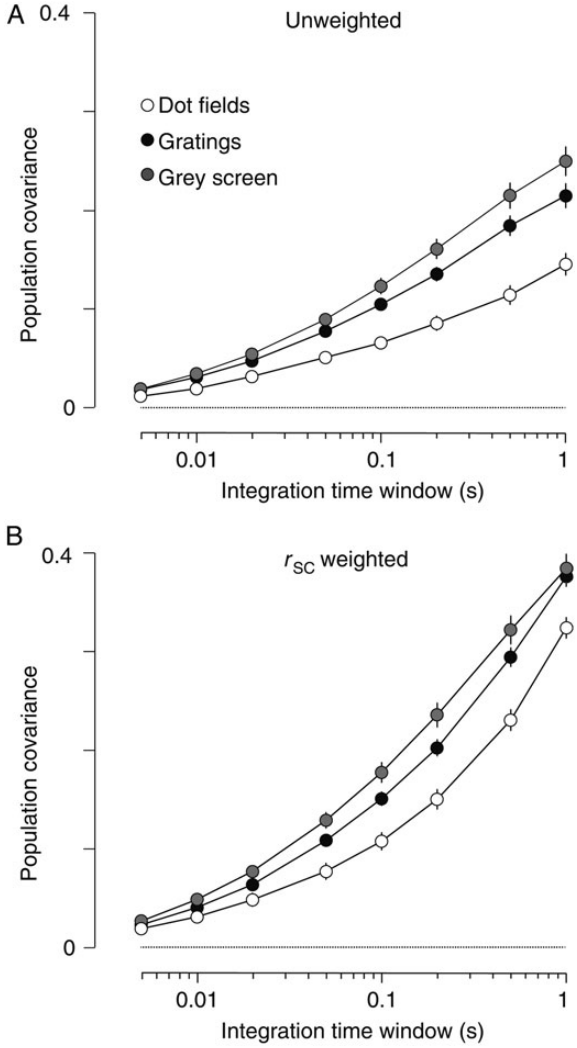

Figure 8. Visual modulation of population covariance. (*A*) Mean population covariance as a function of integration time window, when all neurons in the population were given equal weights, during presentation of moving dot fields (open circles, $n = 151$), moving gratings (black circles, $n = 114$), and a gray screen presented between trials of moving gratings (gray circle, $n = 114$). (*B*) Same as (*A*) but when neural contributions to population response were weighted by the pair-wise noise correlation with the target neuron, r_{SC}. Same neurons as in (*A*).

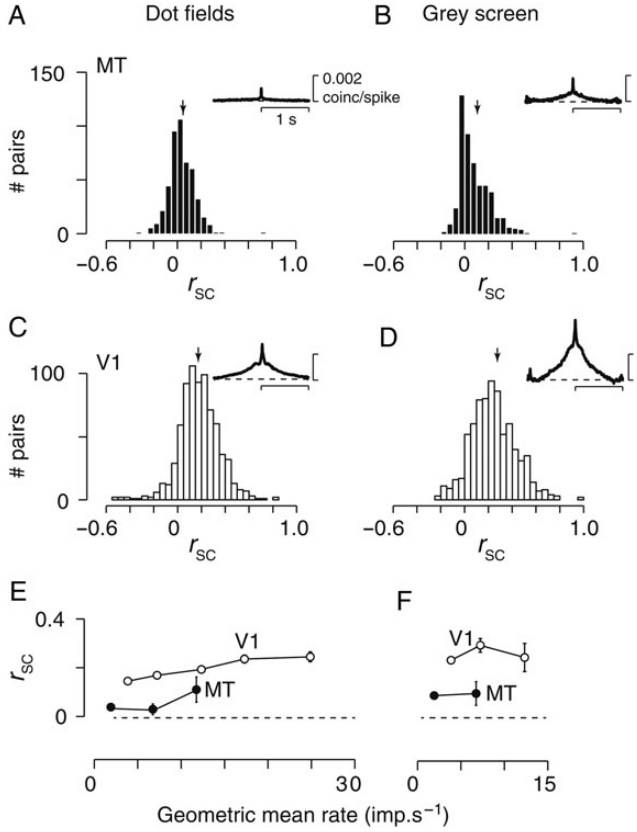

Figure 9. Correlations are lower in area MT than in area V1. (*A*) Distribution of spike count correlation (r_{SC}) in area MT during presentation of a moving dot field. Recordings were obtained with laminar probes and include all neurons that passed response criterion. Arrow shows mean r_{SC} across all pairs ($n = 483$). The inset shows the mean CCG across the same neurons. Scale bars are 1 s (abscissa) and 0.002 coincidences/spike (ordinate). For display purposes, CCGs were smoothed with a Gaussian filter (SD 0.005 s). (*B*) Same as (*A*) but during presentation of a gray screen. Same neurons as (*A*). (*C*,*D*) Same as (*A*,*B*) but for pairs of neurons ($n = 756$) obtained from laminar probes implanted into area V1. (*E*) Mean r_{SC} as a function of geometric mean spike rate for pairs of neurons in area V1 (open circles) and area MT (filled circles). The stimulus was a moving dot field. (*F*) Same as (*E*) but during presentation of a gray screen.

than for neurons in area V1 ($P < 0.001$), but this is because in these experiments firing rate was generally lower in area MT: restricting the comparison to neurons in V1 that had firing rates no greater than those in area MT removed the difference between area MT and area V1 (dot fields: $P = 0.24$, grating: $P = 0.55$; Student's *t*-test).

In summary, noise correlations in area MT are lower than in area V1, and the reduction in r_{SC} is accompanied by lower variability in the activity of individual neurons. In contrast to area MT, correlations are lower for gratings than dot fields in V1.

Discussion

Our study demonstrates that noise correlations in area MT of marmoset are weaker than those in area V1 and depend on both the functional properties of neurons and the visual stimulus. Temporal analyses suggest that these noise correlations comprise distinct components: fast correlations, with timescales 0.05 s or less, that are largely unaffected by visual stimulus, and slower correlations that are dependent on stimulus.

Comparison with Macaque

Previous studies in area MT of awake macaques, using single or closely spaced electrodes, report average r_{SC} between 0.08 and 0.15 during presentation of moving dot fields (Bair et al. 2001; Cohen and Newsome 2009; Huang and Lisberger 2009; Cohen and Kohn 2011). Among pairs of neurons separated by 0.4 mm or less, our estimate of average r_{SC} for dot fields is 0.11. Our measurements show that r_{SC} is greater among pairs of neurons that have similar preferred directions and overlapping receptive fields. These observations extend previous observations, from much smaller samples, in area MT of macaque (de Oliveira et al. 1997; Huang and Lisberger 2009). In addition, we find weak correlations at long timescales that extend over great distances and appear largely independent of functional properties. These appear to reflect large-scale modulation of neuronal activity and may have been invisible to the small samples in previous work.

Previous studies in area V1 of macaque report average r_{SC} between 0.16 and 0.26, usually measured during presentation of drifting gratings (Reich et al. 2001; Kohn and Smith 2005; Gutnisky and Dragoi 2008; Poort and Roelfsema 2009; Samonds et al. 2009; Rasch et al. 2011; Hansen et al. 2012; but see Ecker et al. 2010); reviewed by Cohen and Kohn (2011). Among pairs of neurons in area V1, our estimate of average r_{SC} for gratings is 0.16. Our estimate of r_{SC} for maintained activity (0.24) is lower than that reported in macaque V1 (ca. 0.3; [Kohn and Smith 2005; Smith and Kohn 2008]). The measurements in macaque were made during long periods (15–30 min) of uninterrupted gray screen presentations, whereas the measurements here were made between presentations of visual stimulation. Intermittent visual stimulation may interrupt cortical state and mask slow correlations in spontaneous activity.

In V1, our estimate of r_{SC} during presentation of dot fields was higher than that for gratings; we are not aware of any previous measurements of r_{SC} during presentation of dot fields in area V1. One explanation is that the contrast energy of dot fields is spread across a wide spectrum of spatiotemporal frequencies, and dot fields are therefore effectively low-contrast stimuli for area V1; in macaque V1, r_{SC} is higher when gratings are of low contrast (Kohn and Smith 2005). Alternatively, higher r_{SC} during presentation of dot fields may reflect lower independent variability of V1 neurons, and indeed the Fano Factors of individual V1 neurons were lower during presentation of dot fields than gratings. Reduction in independent variability may unmask shared variability in the activity of pairs of neurons. One or both of these factors may underlie the lower r_{SC} observed for gratings than dots in V1.

Potential Impact of Anesthesia and Array Insertion

Our measurements were made during anesthesia, which was maintained by sufentanil. Anesthesia may have an impact on the spatiotemporal structure of correlations. Our measurements of r_{SC} in area MT are, however, similar to that reported for waking macaque (Zohary et al. 1994; Bair et al. 2001; Cohen and Newsome 2009; Huang and Lisberger 2009). In addition, measurements of r_{SC} in V1 of macaque are similar under sufentanil-anesthesia (Reich et al. 2001; Kohn and Smith 2005; Smith and Kohn 2008) and in waking animals (Samonds et al. 2009; Hansen et al. 2012); our estimates of r_{SC} in V1 of marmoset are similar to that reported for macaque. A second concern is that insertion of large electrode arrays, particularly pneumatic insertion of the 10 × 10 array, is associated with disturbances to the cortical network. In other experiments not shown, we made measurements from tetrodes in area MT of marmoset (Solomon et al. 2011). In that work, we measured response to rapid (duration 0.32 s) serial presentations of dot fields moving in each of 12 directions; the size and speed of the dot fields were tailored to the neurons under study. Pairs of neurons identified in these recordings showed mean r_{SC} of 0.12 (SEM 0.02; 99 pairs from 7 animals). We conclude that our estimates of correlation are unlikely to be distorted by insertion of the recording arrays.

Propagation of Noise Correlations along Visual Hierarchy

r_{SC} is on average weak in marmoset LGN, particularly in parvocellular and magnocellular layers (Cheong et al. 2011); r_{SC} is also weak in the input layers of macaque area V1 (Hansen et al. 2012; Smith et al. 2013). Throughout most of macaque V1 and V2, however, r_{SC} is on average positive, in the range of 0.1 to 0.3, and extends over large distances and across very different receptive field preferences (Smith and Kohn 2008; Hansen et al. 2012; Smith et al. 2013). This is in accord with our measurements of r_{SC} in V1 of marmoset. Our measurements do show that pairs of neurons in area MT recorded from the same electrode, with the same direction preference, can show r_{SC} as high as those measured in V1, but r_{SC} in area MT decays rapidly with cortical distance and functional dissimilarity. Our measurements therefore agree with meta-analysis of research in macaque, which suggests that overall r_{SC} in area V1 is higher than in area MT (Cohen and Kohn 2011). Those studies, however, were conducted under a range of conditions. One advantage of our study is that it allows direct comparison of correlations in the 2 areas: the visual stimuli, recording, analysis and anesthesia were the same for measurements from both areas. We cannot rule out the possibility that lower r_{SC} in area MT reflects an additional effect of anesthesia on network properties in area MT, but the parsimonious explanation of our own measurements and those of others is that correlations are weaker in area MT than in area V1. Sequential reduction in noise correlation may be a general rule in visual cortex: r_{SC} in area MSTd of macaque, which draws substantial input from area MT, is on average low and may be zero (Gu et al. 2011; Liu et al. 2013).

If neurons in area MT simply summed the input of many V1 afferents, then r_{SC} in area MT should be higher than in V1. This is because summing inputs averages out variability that is not shared: the activity of each neuron in area MT will be dominated by the activity that is common among the afferent neurons. The broad spread of r_{SC} throughout area V1 means that even if pairs of neurons in area MT drew input from non-overlapping pools of V1 afferents, r_{SC} should still be larger in area MT than area V1. Why then are correlations generally lower in area MT than area V1? One explanation may be that additional feed-forward input to area MT, which arises in areas V2, V3, LGN, and pulvinar (Maunsell and van Essen 1983; Palmer and Rosa 2006), dilutes correlations propagated from area V1. Indeed, neurons in area MT can remain visually responsive, and direction-tuned, in the absence of area V1 (Rodman et al. 1989; Girard et al. 1992; Rosa et al. 2000). If response variability in these other areas is not correlated with that in area V1, then correlations may be lower in area MT than area V1.

Additionally, inhibition or suppression within area MT may be important in reducing correlations that would otherwise be inherited from V1. Co-variation of excitation and inhibition helps decorrelate neuronal activity (Graupner and Reyes 2013), and it is generally thought that neurons in area MT draw on both excitatory and inhibitory inputs to build receptive fields (Rust et al. 2006). This idea is attractive because the broad spread of r_{SC} in area V1 introduces redundancy to the activity of those neurons. It is well established that inhibition and suppression, through for example center-surround receptive fields or gain control mechanisms, can help reduce redundancy in sensory signals (Attneave 1954; Barlow 1961; Srinivasan et al. 1982; Schwartz and Simoncelli 2001). In particular, a center-surround receptive field provides an efficient and accurate decoding mechanism in the presence of widespread correlated variability (Chen et al. 2006, 2008), such as that observed in V1.

Stimulus-Dependence of Correlations in Area MT

The primary impact of visual stimulation on correlations in area MT was a reduction in slow correlations, those with timescales longer than 0.05 s. The stimulus-dependent reduction in correlations is consistent with the idea that visual stimulation stabilizes neuronal networks (Nowak et al. 1999; Monier et al. 2003; Finn et al. 2007; Smith and Kohn 2008; Kohn et al. 2009; Churchland et al. 2010), although the mechanism(s) that allow this stabilization are unclear. In addition, we find that r_{SC} is weaker during presentation of dot fields than during presentation of gratings, and more dependent on the similarity of receptive fields. Again these differences predominantly reflect reduced correlation at timescales above 0.05 s. Lower correlations during presentation of dot fields may have functional implications, as follows. Noise correlations among neurons in area MT can account for the variation in speed and direction of smooth pursuit eye movements (Huang and Lisberger 2009). Our observations suggest that pursuit should be less precise for gratings than for dot fields, consistent with reports that pursuit of narrowband stimuli is less precise than broadband stimuli (Simoncini et al. 2012). Following the logic mentioned earlier, lower correlations during presentation of dot fields may reflect stronger inhibition or suppression in area MT for dot fields than gratings, whether that inhibition arises from within or outside the classical receptive field (Snowden et al. 1991; Simoncelli and Heeger 1998; Rust et al. 2006; Hunter and Born, 2011; Allman et al. 1985; Lui et al. 2007).

Unlike for slower correlations, the distribution and magnitude of near-synchronous activity, particularly evidenced by analysis of jitter-corrected CCGs, was similar during presentation of a gray screen, dot fields, and gratings. This suggests that near-synchronous activity arises from direct connectivity, either between constituent neurons, or through shared inputs, that is not modified by slower changes in neuronal sensitivity. In addition to this near-synchronous activity, shuffle-corrected CCGs obtained during presentation of drifting gratings showed sharp peaks that persisted across the breadth of area MT. These peaks may reflect presence of high frequency (gamma-band) coherence: preliminary analysis of local field potentials from area MT of marmoset shows increase in gamma-band coherence during presentation of gratings but not dot fields (Solomon SS and Solomon SG, unpublished observations). This gamma-band coherence may arise in area MT or be propagated from area V1 (Bartolo et al. 2011; Jia et al. 2011).

We do not know whether or how feedback to area MT (Maunsell and van Essen 1983) contributes to the spatio-temporal distribution of spike correlations. Nor do we know whether feedback from extrastriate areas, including area MT, contributes to long-distance correlations in activity of V1 neurons (Smith and Kohn 2008). If feedback from area MT does contribute to long-distance correlations in V1, then those correlations may show similar dependence on visual stimulus, and this might be a productive target of future work.

Supplementary Material

Supplementary material can be found at: http://www.cercor.oxfordjournals.org/.

Funding

This work was supported by National Health & Medical Research Council of Australia (NHMRC) Grant 1005427, and by the ARC Centre of Excellence in Vision Science.

Notes

We thank C. Davey, S.K. Cheong, A. Pietersen, P. Romo, and N. Zeater for help in collecting the data and A. Kohn and P.R. Martin for comments on previous versions of this manuscript. *Conflict of Interest*: None declared.

References

Allman J, Miezin F, McGuinness E. 1985. Direction- and velocity-specific responses from beyond the classical receptive field in the middle temporal visual area (MT). Perception. 14:105–126.

Amarasingham A, Harrison MT, Hatsopoulos NG, Geman S. 2012. Conditional modeling and the jitter method of spike resampling. J Neurophysiol. 107:517–531.

Attneave F. 1954. Some informational aspects of visual perception. Psychol Rev. 61:183–193.

Bair W, Zohary E, Newsome WT. 2001. Correlated firing in macaque visual area MT: time scales and relationship to behavior. J Neurosci. 21:1676–1697.

Barlow HB. 1961. Possible principles underlying the transformation of sensory messages. In: Rosenblith W, editor. Sensory Communication. M.I.T. Press p. 217–234.

Bartolo MJ, Gieselmann MA, Vuksanovic V, Hunter D, Sun L, Chen X, Delicato LS, Thiele A. 2011. Stimulus-induced dissociation of neuronal firing rates and local field potential gamma power and its relationship to the resonance blood oxygen level-dependent signal in macaque primary visual cortex. Eur J Neurosci. 34:1857–1870.

Born RT, Bradley DC. 2005. Structure and function of visual area MT. Annu Rev Neurosci. 28:157–189.

Bourne JA, Warner CE, Upton DJ, Rosa MG. 2007. Chemoarchitecture of the middle temporal visual area in the marmoset monkey (*Callithrix jacchus*): laminar distribution of calcium-binding proteins (calbindin, parvalbumin) and nonphosphorylated neurofilament. J Comp Neurol. 500:832–849.

Britten KH, Shadlen MN, Newsome WT, Movshon JA. 1992. The analysis of visual motion: a comparison of neuronal and psychophysical performance. J Neurosci. 12:4745–4765.

Chen A, Deangelis GC, Angelaki DE. 2013. Functional specializations of the ventral intraparietal area for multisensory heading discrimination. J Neurosci. 33:3567–3581.

Chen Y, Geisler WS, Seidemann E. 2006. Optimal decoding of correlated neural population responses in the primate visual cortex. Nat Neurosci. 9:1412–1420.

Chen Y, Geisler WS, Seidemann E. 2008. Optimal temporal decoding of neural population responses in a reaction-time visual detection task. J Neurophysiol. 99:1366–1379.

Cheong SK, Tailby C, Martin PR, Levitt JB, Solomon SG. 2011. Slow intrinsic rhythm in the koniocellular visual pathway. Proc Natl Acad Sci USA. 108:14659–14663.

Cheong SK, Tailby C, Solomon SG, Martin PR. 2013. Cortical-like receptive fields in the lateral geniculate nucleus of marmoset monkeys. J Neurosci. 33:6864–6876.

Churchland MM, Yu BM, Cunningham JP, Sugrue LP, Cohen MR, Corrado GS, Newsome WT, Clark AM, Hosseini P, Scott BB et al.. 2010. Stimulus onset quenches neural variability: a widespread cortical phenomenon. Nat Neurosci. 13:369–378.

Cohen MR, Kohn A. 2011. Measuring and interpreting neuronal correlations. Nat Neurosci. 14:811–819.

Cohen MR, Newsome WT. 2009. Estimates of the contribution of single neurons to perception depend on timescale and noise correlation. J Neurosci. 29:6635–6648.

de la Rocha J, Doiron B, Shea-Brown E, Josic K, Reyes A. 2007. Correlation between neural spike trains increases with firing rate. Nature. 448:802–806.

de Oliveira SC, Thiele A, Hoffmann KP. 1997. Synchronization of neuronal activity during stimulus expectation in a direction discrimination task. J Neurosci. 17:9248–9260.

Ecker AS, Berens P, Tolias AS, Bethge M. 2010. The effect of noise correlations in populations of diversely tuned neurons. J Neurosci. 31:14272–14283.

Finn IM, Priebe NJ, Ferster D. 2007. The emergence of contrast-invariant orientation tuning in simple cells of cat visual cortex. Neuron. 54:137–152.
Girard P, Salin PA, Bullier J. 1992. Response selectivity of neurons in area MT of the macaque monkey during reversible inactivation of area V1. J Neurophysiol. 67:1437–1446.
Graupner M, Reyes AD. 2013. Synaptic input correlations leading to membrane potential decorrelation of spontaneous activity in cortex. J Neurosci. 33:15075–15085.
Gu Y, Liu S, Fetsch CR, Yang Y, Fok S, Sunkara A, DeAngelis GC, Angelaki DE. 2011. Perceptual learning reduces interneuronal correlations in macaque visual cortex. Neuron. 71:750–761.
Gutnisky DA, Dragoi V. 2008. Adaptive coding of visual information in neural populations. Nature. 452:220–224.
Hansen BJ, Chelaru MI, Dragoi V. 2012. Correlated variability in laminar cortical circuits. Neuron. 76:590–602.
Hata Y, Tsumoto T, Sato H, Tamura H. 1991. Horizontal interactions between visual cortical neurones studied by cross-correlation analysis in the cat. J Physiol. 441:593–614.
Huang X, Lisberger SG. 2009. Noise correlations in cortical area MT and their potential impact on trial-by-trial variation in the direction and speed of smooth-pursuit eye movements. J Neurophysiol. 101:3012–3030.
Hunter JN, Born RT. 2011. Stimulus-dependent modulation of suppressive influences in MT. J Neurosci. 31:678–686.
Jia X, Smith MA, Kohn A. 2011. Stimulus selectivity and spatial coherence of gamma components of the local field potential. J Neurosci. 31:9390–9403.
Kelly RC, Smith MA, Samonds JM, Kohn A, Bonds AB, Movshon JA, Lee TS. 2007. Comparison of recordings from microelectrode arrays and single electrodes in the visual cortex. J Neurosci. 27:261–264.
Kohn A, Smith MA. 2005. Stimulus dependence of neuronal correlation in primary visual cortex of the macaque. J Neurosci. 25: 3661–3673.
Kohn A, Zandvakili A, Smith MA. 2009. Correlations and brain states: from electrophysiology to functional imaging. Curr Opin Neurobiol. 19:434–438.
Liu S, Gu Y, DeAngelis GC, Angelaki DE. 2013. Choice-related activity and correlated noise in subcortical vestibular neurons. Nat Neurosci. 16:89–97.
Lui LL, Bourne JA, Rosa MG. 2007. Spatial summation, end inhibition and side inhibition in the middle temporal visual area (MT). J Neurophysiol. 97:1135–1148.
Lyon DC, Nassi JJ, Callaway EM. 2010. A disynaptic relay from superior colliculus to dorsal stream visual cortex in macaque monkey. Neuron. 65:270–279.
Maunsell JH, van Essen DC. 1983. The connections of the middle temporal visual area (MT) and their relationship to a cortical hierarchy in the macaque monkey. J Neurosci. 3:2563–2586.
McDonald JS, Clifford CW, Solomon SS, Chen SC, Solomon SG. 2014. Integration and segregation of multiple motion signals by neurons in area MT of primate. J Neurophysiol. 111:369–378.
Monier C, Chavane F, Baudot P, Graham LJ, Fregnac Y. 2003. Orientation and direction selectivity of synaptic inputs in visual cortical neurons: a diversity of combinations produces spike tuning. Neuron. 37:663–680.
Moore GP, Segundo JP, Perkel DH, Levitan H. 1970. Statistical signs of synaptic interaction in neurons. Biophys J. 10:876–900.
Muller JR, Metha AB, Krauskopf J, Lennie P. 2001. Information conveyed by onset transients in responses of striate cortical neurons. J Neurosci. 21:6978–6990.
Nassi JJ, Lyon DC, Callaway EM. 2006. The parvocellular LGN provides a robust disynaptic input to the visual motion area MT. Neuron. 50:319–327.
Nelson JI, Salin PA, Munk MH, Arzi M, Bullier J. 1992. Spatial and temporal coherence in cortico-cortical connections: a cross-correlation study in areas 17 and 18 in the cat. Vis Neurosci. 9:21–37.
Newsome WT, Britten KH, Movshon JA. 1989. Neuronal correlates of a perceptual decision. Nature. 341:52–54.
Newsome WT, Pare EB. 1988. A selective impairment of motion perception following lesions of the middle temporal visual area (MT). J Neurosci. 8:2201–2211.
Nordhausen CT, Maynard EM, Normann RA. 1996. Single unit recording capabilities of a 100 microelectrode array. Brain Res. 726:129–140.
Nowak LG, Munk MH, James AC, Girard P, Bullier J. 1999. Cross-correlation study of the temporal interactions between areas V1 and V2 of the macaque monkey. J Neurophysiol. 81:1057–1074.
Nowak LG, Munk MH, Nelson JI, James AC, Bullier J. 1995. Structural basis of cortical synchronization. I. Three types of interhemispheric coupling. J Neurophysiol. 74:2379–2400.
Palmer SM, Rosa MG. 2006. Quantitative analysis of the corticocortical projections to the middle temporal area in the marmoset monkey: evolutionary and functional implications. Cereb Cortex. 16:1361–1375.
Poort J, Roelfsema PR. 2009. Noise correlations have little influence on the coding of selective attention in area V1. Cereb Cortex. 19:543–553.
Priebe NJ, Lisberger SG. 2004. Estimating target speed from the population response in visual area MT. J Neurosci. 24:1907–1916.
Rasch MJ, Schuch K, Logothetis NK, Maass W. 2011. Statistical comparison of spike responses to natural stimuli in monkey area V1 with simulated responses of a detailed laminar network model for a patch of V1. J Neurophysiol. 105:757–778.
Reich DS, Mechler F, Victor JD. 2001. Independent and redundant information in nearby cortical neurons. Science. 294:2566–2568.
Rodman HR, Gross CG, Albright TD. 1989. Afferent basis of visual response properties in area MT of the macaque. I. Effects of striate cortex removal. J Neurosci. 9:2033–2050.
Rosa MG, Elston GN. 1998. Visuotopic organisation and neuronal response selectivity for direction of motion in visual areas of the caudal temporal lobe of the marmoset monkey (*Callithrix jacchus*): middle temporal area, middle temporal crescent, and surrounding cortex. J Comp Neurol. 393:505–527.
Rosa MG, Tweedale R, Elston GN. 2000. Visual responses of neurons in the middle temporal area of new world monkeys after lesions of striate cortex. J Neurosci. 20:5552–5563.
Rousche PJ, Normann RA. 1992. A method for pneumatically inserting an array of penetrating electrodes into cortical tissue. Ann Biomed Eng. 20:413–422.
Rust NC, Mante V, Simoncelli EP, Movshon JA. 2006. How MT cells analyze the motion of visual patterns. Nat Neurosci. 9:1421–1431.
Salzman CD, Britten KH, Newsome WT. 1990. Cortical microstimulation influences perceptual judgements of motion direction. Nature. 346:174–177.
Samonds JM, Potetz BR, Lee TS. 2009. Cooperative and competitive interactions facilitate stereo computations in macaque primary visual cortex. J Neurosci. 29:15780–15795.
Schwartz O, Simoncelli EP. 2001. Natural signal statistics and sensory gain control. Nat Neurosci. 4:819–825.
Shadlen MN, Newsome WT. 1998. The variable discharge of cortical neurons: implications for connectivity, computation, and information coding. J Neurosci. 18:3870–3896.
Simoncelli EP, Heeger DJ. 1998. A model of neuronal responses in visual area MT. Vision Res. 38:743–761.
Simoncini C, Perrinet LU, Montagnini A, Mamassian P, Masson GS. 2012. More is not always better: adaptive gain control explains dissociation between perception and action. Nat Neurosci. 15: 1596–1603.
Sincich LC, Park KF, Wohlgemuth MJ, Horton JC. 2004. Bypassing V1: a direct geniculate input to area MT. Nat Neurosci. 7:1123–1128.
Smith MA, Jia X, Zandvakili A, Kohn A. 2013. Laminar dependence of neuronal correlations in visual cortex. J Neurophysiol. 109:940–947.
Smith MA, Kohn A. 2008. Spatial and temporal scales of neuronal correlation in primary visual cortex. J Neurosci. 28:12591–12603.
Smith MA, Sommer MA. 2013. Spatial and temporal scales of neuronal correlation in visual area V4. J Neurosci. 33:5422–5432.
Snider RK, Kabara JF, Roig BR, Bonds AB. 1998. Burst firing and modulation of functional connectivity in cat striate cortex. J Neurophysiol. 80:730–744.
Snowden RJ, Treue S, Erickson RG, Andersen RA. 1991. The response of area MT and V1 neurons to transparent motion. J Neurosci. 11:2768–2785.

Solomon SG, White AJ, Martin PR. 2002. Extraclassical receptive field properties of parvocellular, magnocellular, and koniocellular cells in the primate lateral geniculate nucleus. J Neurosci. 22:338–349.
Solomon SS, Tailby C, Gharaei S, Camp AJ, Bourne JA, Solomon SG. 2011. Visual motion integration by neurons in the middle temporal area of a New World monkey, the marmoset. J Physiol. 589: 5741–5758.
Srinivasan MV, Laughlin SB, Dubs A. 1982. Predictive coding: a fresh view of inhibition in the retina. Proc R Soc Lond B Biol Sci. 216: 427–459.
Suner S, Fellows MR, Vargas-Irwin C, Nakata GK, Donoghue JP. 2005. Reliability of signals from a chronically implanted, silicon-based electrode array in non-human primate primary motor cortex. IEEE Trans Neural Syst Rehabil Eng. 13:524–541.
van Kan PL, Scobey RP, Gabor AJ. 1985. Response covariance in cat visual cortex. Exp Brain Res. 60:559–563.
Warner CE, Goldshmit Y, Bourne JA. 2010. Retinal afferents synapse with relay cells targeting the middle temporal area in the pulvinar and lateral geniculate nuclei. Front Neuroanat. 4:8.
Weller RE, Wall JT, Kaas JH. 1984. Cortical connections of the middle temporal visual area (MT) and the superior temporal cortex in owl monkeys. J Comp Neurol. 228:81–104.
White AJ, Solomon SG, Martin PR. 2001. Spatial properties of koniocellular cells in the lateral geniculate nucleus of the marmoset *Callithrix jacchus*. J Physiol. 533:519–535.
Yu HH, Verma R, Yang Y, Tibballs HA, Lui LL, Reser DH, Rosa MG. 2010. Spatial and temporal frequency tuning in striate cortex: functional uniformity and specializations related to receptive field eccentricity. Eur J Neurosci. 31:1043–1062.
Zohary E, Shadlen MN, Newsome WT. 1994. Correlated neuronal discharge rate and its implications for psychophysical performance. Nature. 370:140–143.